Self-propulsion in a low-Reynolds-number fluid confined by two walls of a microchannel

Ali Najafi,* Seyede Somaye Hoseini Raad, and Roghaye Yousefi
Physics Department, University of Zanjan, Zanjan 313, Iran
(Received 10 June 2013; revised manuscript received 7 August 2013; published 3 October 2013)

The problem of hydrodynamic interactions with confining walls is examined for a model of a microswimmer composed of three connected beads. Two parallel walls of a narrow microfluidic channel confine the fluid flow. We show that different trajectories for this linear swimmer emerge because of long-range hydrodynamic interactions with the walls of the channel. The possibility of space-spanning trajectories for this swimmer can potentially introduce it as a candidate for constructing a mixing device for working at the laminar flow conditions in microfluidic channels.

DOI: 10.1103/PhysRevE.88.045001 PACS number(s): 47.63.mf, 07.10.Cm, 87.19.ru

I. INTRODUCTION

Dissipation-dominated dynamics of a fluid medium on a micrometer scale is an old but still interesting area in physics [1–3]. Because of the hydrodynamic peculiarity in the low Reynolds condition, the study of propulsion mechanisms and pumping methods in this condition has attracted a great deal of interest recently [4]. Studying and understanding the dynamics of swimming micro-organisms and artificial microswimmers are important motivations for such studies. In the case of swimming micro-organisms, it is a well known fact that long-range hydrodynamic interactions with confining walls will lead to a class of interesting phenomena [5–10]. The attraction and consequent adhesion of certain individual micro-organisms to surfaces in biofilms [11], the boundary effects on the dynamics of swimming suspensions [12], and the large circular trajectories for *E. coli* in the presence of walls [7,13] are among the biologically relevant examples.

In addition to the physics of swimming micro-organisms, applications of artificial swimmers in microfluidic experiments are also interesting [14–16]. In these systems, one needs to increase the rate of chemical reactions by mixing the components [17,18]. Laminar flow at the microfluidic channels does not allow turbulent mixing of the liquid. On the other hand, the large time scale of the diffusion process, i.e., the fluctuation-based mixing mechanism, makes it impractical at the micrometer scale. Passive and active scenarios have been proposed to enhance the diffusion process and subsequently increase the mixing efficiency [19]. Periodic stretching and folding the flow inside a channel increase passively the interface between the inlet flows and provide a greater opportunity for mixing [20]. Energy injection into the system through actuating magnetic colloids [21,22], artificial cilia, bubbles, etc., is among the active methods for achieving rapid mixing [23–25].

In this article, we theoretically study the dynamics of a microswimmer inside a channel that can be an active mixing device. Among all the proposed molecular machines [27–29], we study the simplest one. Our system is made up of a collection of three micron-scale beads manipulated by external forces. The hydrodynamics of this model, without taking into account any confining effects, has been studied previously [30,31]. It is theoretically and experimentally shown that the three-bead system can either work in swimming or pumping mode [26]. A single confining wall has been investigated before [6]; two-wall confinement shows a number of interesting behaviors.

II. RESULTS

We consider the three-bead swimmer consisting of three rigid microspheres of equal radii a that are aligned linearly by means of external forces. The average distances between the adjacent beads are fixed to ℓ. As shown in Fig. 1, the swimmer is located in the (x,z) plane and its direction is denoted by a unit vector $\hat{\mathbf{t}}$. To complete the mathematical description of the kinematics, we denote the position vectors of the spheres by $\mathbf{r}_\alpha$, with $\alpha \in \{M,R,L\}$ denoting the middle, right, and left beads.

To model a microfluidic channel, we consider a special and simplified case in which the fluid is confined between two infinite and parallel walls. Two rigid, parallel, and no-slip walls are placed at positions $z = 0$ and $z = H$. The internal motion of the swimmer that can be induced by external fields is given by the following constraints:

$$\mathbf{r}_{R,L} = \mathbf{r}_M \pm [\ell + u\cos(\omega t + \phi_{R,L})]\hat{\mathbf{t}}. \tag{1}$$

Here u, ω, and $\phi_{R,L}$ stand for the amplitude, frequency, and phases for the internal motion. In the case of experimental realization, three different optical tweezers manipulate the bead position [26]. We study the problem at a very low value of dimensionless Reynolds number $\mathcal{R}e = \rho\ell u\omega/\eta$, where ρ and η show the density and viscosity of the fluid [32]. This is the condition of a microfluidic medium [14]. Because of the symmetry considerations and neglecting thermal orientational fluctuations, we can quickly conclude that the initial director of the swimmer and a unit vector perpendicular to the walls will construct a two-dimensional plane [here an $(x$-$z)$ plane] inside which the motion should take place.

For a very wide channel, $H \gg \ell$, and a swimmer moving near the middle of the channel, $z \approx H/2$, the walls have no perceivable hydrodynamic effects on the swimmer, and the swimmer continues on its initial orientation. Considering the case in which $u \ll \ell$, the average velocity of the swimmer and the average hydrodynamic forces applied on the beads are

*najafi@znu.ac.ir

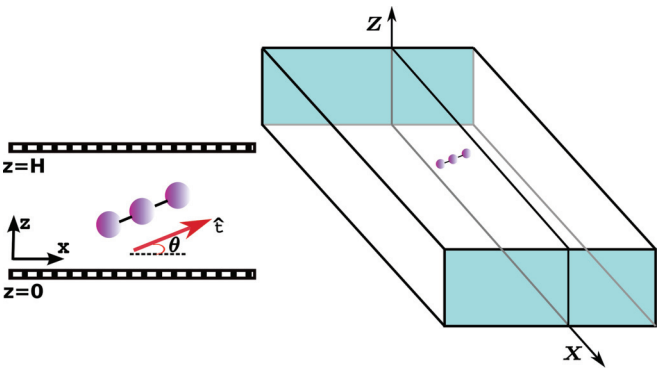

FIG. 1. (Color online) The geometry of a microfluidic channel and a low Reynolds number three-sphere swimmer. We assume that the channel is wide and long so that only the effects of two upper and lower walls of the channel are considered.

given by [31]

$$\langle \dot{\mathbf{r}}_M \rangle = \mathcal{V}\hat{\mathbf{t}}, \quad \mathbf{f}_R = \mathbf{f}_L = -(1/2)\mathbf{f}_M = \tfrac{15}{7}\pi\eta a\mathcal{V}\hat{\mathbf{t}}, \qquad (2)$$

where the unit vector $\hat{\mathbf{t}}$ shows the direction of this linear swimmer and $\mathcal{V} = (7/24)(u^2/\ell^2)a\omega\sin(\phi_L - \phi_R)$. An immediate and interesting conclusion from Eq. (2) is that the self-propulsion is possible only when a nonzero phase lag between the two lateral distances is applied. This is the content of Purcell's famous scallop theorem [1].

However, inside a channel, the backscattering of the fluid flow from the walls dynamically changes the velocity and orientation of the swimmer. As a result of the initial conditions of the swimmer, the scattered flow can have different effects on the swimmer. Figure 2 summarizes the results of our

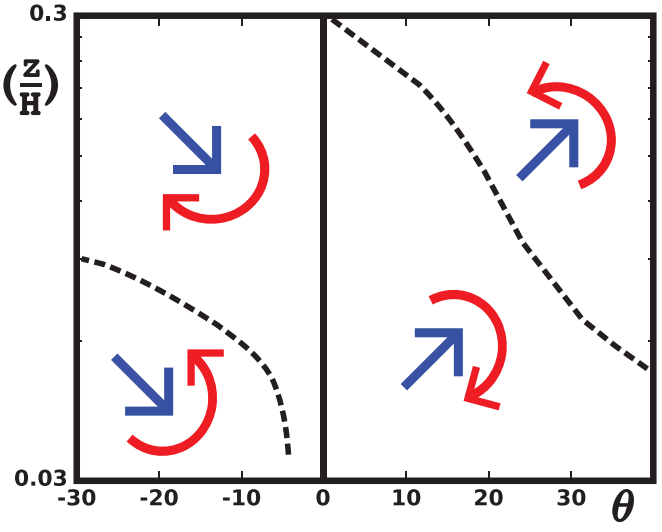

FIG. 2. (Color online) A phase diagram representing the overall hydrodynamic influences of a microchannel on a microswimmer. Thick (blue) arrows show the intrinsic direction of the swimmer while curved arrows (red) show the rotational velocities due to the interaction with walls. No other phase changes occur at the omitted parts of the phase diagram. The geometrically inaccessible region of the phase diagram ($z/\ell < \sin\theta$) is not shown in this logarithmic scale. The numerical parameters are $H/\ell = 30$, $u/\ell = a/\ell = 0.4$, $(\phi_L - \phi_R) = \pi/2$, and $\omega = 1$.

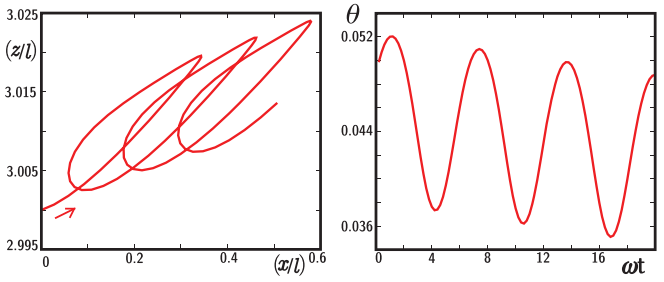

FIG. 3. (Color online) An example showing the trajectory of a swimmer interacting with two walls of a microchannel. Numerical parameters are similar to Fig. 2.

numerical integration of the dynamical equations of motion for a swimmer moving inside the channel and interacting with the walls. In this phase diagram, the horizontal axis denotes the initial angle θ that the swimmer's direction makes with the x axis ($\cos\theta = \hat{\mathbf{t}} \cdot \hat{\mathbf{x}}$), and the vertical axis shows the initial perpendicular distance between the swimmer (middle bead) and the wall located at $z = 0$. The straight arrows show the velocity direction and the curved arrows mimic the rotational velocity of the swimmer. At small z, the hydrodynamic effects of the lower wall dominate, while at large z ($z \approx H/2$) the effects due to both walls are presented. In either case, i.e., motion near the walls of the channel or motion near the middle of the channel, the hydrodynamic interactions have a tendency to separate different swimmers that have positive and negative directions by reorienting them to different directions.

In this phase diagram, we have studied the cases with the initial direction in the interval $-\pi/2 < \theta < \pi/2$. The case with $0 < \theta < \pi/2$ corresponds to a swimmer that initially starts to move toward the middle of the channel, while $-\pi/2 < \theta < 0$ represents the motion toward the nearby wall. As one can see from this phase diagram, clockwise and counterclockwise tendencies for rotation due to the channel's effects depend strongly on the initial position and orientation of the system.

As an example, Fig. 3 shows the trajectory of a swimmer that has a positive but small initial angle and that is located near the lower wall ($z = 0$) of the channel. Here $\theta > 0$ and $\mathcal{V} > 0$ mean that the swimmer is moving toward the middle of the channel. The orientational dynamics of the swimmer shows two timing characteristics, namely short-time oscillations and nontrivial long-time behavior. The short-time oscillation is mainly due to the forcing mechanism that makes the system active. The average- and long-time orientation of this example swimmer change in the clockwise direction to eventually make the swimmer parallel to the walls ($\theta = 0$).

A very interesting feature of the trajectories of swimming inside the channel is reflected in the above example: the trajectory has an oscillatory and space-scanning feature. It is interesting that an active but linear swimmer changes its direction periodically and navigates in such a way that it can scan a finite area inside the fluid. This capability emerges essentially because of the presence of channel walls. It is reasonable to expect that the oscillatory nature of the swimmer's trajectory may lead to an enhanced mixing. The pumping mode of the three-bead system is also interesting [26]. One can argue that in the pumping mode, the above results are

also applicable. Similar to the case of the swimming mode, here we might expect an enhanced mixing.

III. DETAILS OF THE HYDRODYNAMICS

At the very low $\mathcal{R}e$ condition, the Stokes and the continuity equations govern the dynamics of the fluid. For such a fluid that is under the action of hydrodynamic forces from the beads, we can write the Stokes and continuity equations as

$$\eta\nabla^2\mathbf{u}(\mathbf{x}) - \nabla p(\mathbf{x}) = \sum_\alpha \mathbf{f}_\alpha \delta(\mathbf{r}-\mathbf{r}_\alpha), \quad \nabla\cdot\mathbf{u}(\mathbf{x}) = \mathbf{0}, \tag{3}$$

where $\alpha \in \{R,M,L\}$. The velocity of the spheres and the velocity of the fluid satisfy the boundary conditions: $\dot{\mathbf{r}}_\alpha = \mathbf{u}(\mathbf{r}_\alpha)$. We treat the external manipulation mechanism as constraining equations. In this case, the total hydrodynamic forces and torques acting on the whole system should vanish. Here we have assumed that each bead acts as a singular point force. This assumption is valid for very small beads where $a \ll \ell$. Linearity of the Stokes equation leads to linear relations between the velocities and hydrodynamic forces in the following form:

$$u_i(\mathbf{r}) = \sum_\alpha \sum_j O_{ij}^{2w}(\mathbf{r}-\mathbf{r}_\alpha) f_{\alpha,j}, \tag{4}$$

where O^{2w} represents the hydrodynamic interaction tensor. An essential difficulty in this problem comes from the no-slip boundary condition on the walls: $\mathbf{u}(\mathbf{r}\in\text{wall}) = 0$. The superscript $2w$ for the hydrodynamic interaction reflects the fact that the velocity field decays to zero on the walls. As shown by Liron *et al.* [33], the hydrodynamic interaction of a single point force moving between two parallel walls can be constructed by a set of an infinite number of image point forces as

$$O_{ij}^{2w} = \sum_{n=0,\pm1}^{\pm\infty} \left[O_{ij}^0(\mathbf{r}-\mathbf{r}_n^+) - O_{ij}^0(\mathbf{r}-\mathbf{r}_n^-)\right] + \Delta(\mathbf{r}-\mathbf{r}_\alpha), \tag{5}$$

where the unbounded (in the absence of any wall) hydrodynamic interaction tensor in Oseen's approximation is given by $O_{ij}^0(\mathbf{r}) = (\delta_{ij}+\hat{r}_i\hat{r}_j)/(8\pi\eta r)$ [34]. The positions of image sources are given by $\mathbf{r}_n^\pm = \mathbf{r}_\alpha + [2nH + (-1\pm1)z_\alpha]\hat{\mathbf{z}}$, where $z_\alpha = \mathbf{r}_\alpha\cdot\hat{\mathbf{z}}$ is the distance between the point force and the lower wall. Extending the idea of the image source in the case of a single wall [35] to the case of two walls, it is shown in [33] that the series of image forces do not completely satisfy the boundary condition on the walls, and a term Δ is necessary to satisfy the boundary condition; the cumbersome structure of this function is not given here [33]. Numerical integration of the dynamic equations, taking into account the complete and detailed structure of the hydrodynamic interactions, leads us to the trajectories that are summarized in Figs. 2 and 3 and discussed before.

IV. ASYMPTOTIC RESULTS

To gain more insight into the underlying hydrodynamics of the system, we present an asymptotic picture of the system that is valid in the limit of $\ell/H \ll 1$ and $a/\ell \ll 1$. As pointed out before, for a very wide channel (free swimmer), the force distribution for the swimmer moving near the middle of the channel is a force quadrupole as follows:

$$\mathbf{f}(\mathbf{r}) = f[-(1/2)\delta(\mathbf{r}) + \delta(\mathbf{r}-\ell\hat{\mathbf{t}}) + \delta(\mathbf{r}+\ell\hat{\mathbf{t}})]\hat{\mathbf{t}}, \tag{6}$$

where $f = (15/7)\pi\eta a\mathcal{V}$. In the region very far from this free swimmer, the velocity field corresponds to the velocity field of a force quadrupole and is given by [34]

$$u_i^Q(\mathbf{r}) = \sum_{jlm} S_{ijlm}^Q(\mathbf{r}) T_{jlm}, \tag{7}$$

where the quadruple strength and field are given by

$$\begin{aligned} T_{jlm} &= (1/2)\int d\mathbf{r}' f_j r_l' r_m' = f\ell^2 \hat{\mathbf{t}}_j\hat{\mathbf{t}}_l\hat{\mathbf{t}}_m, \\ S_{ijlm}^Q &= (\partial/\partial\mathbf{r}_l)(\partial/\partial\mathbf{r}_m) O_{ij}^0(\mathbf{r}). \end{aligned} \tag{8}$$

Collecting these results, we can write the velocity field of a free swimmer as

$$\mathbf{u}^Q(\mathbf{r}) = \frac{f\ell^2}{8\pi\eta r^3}\{[1-3(\hat{\mathbf{t}}\cdot\hat{\mathbf{r}})^2]\hat{\mathbf{t}} + 3(\hat{\mathbf{t}}\cdot\hat{\mathbf{r}})[5(\hat{\mathbf{t}}\cdot\hat{\mathbf{r}})^2 - 3]\hat{\mathbf{r}}\}. \tag{9}$$

Now to obtain the hydrodynamic influences of the wall, we should solve a Stokes equation for a velocity of the scattered flow $\mathbf{u}^{2w}$ as $\eta\nabla^2\mathbf{u}^{2w} - \nabla p^{2w} = \mathbf{0}$. The scattered flow is subject to the following boundary condition: $\mathbf{u}^{2w}(\mathbf{r}_{2w}) = -\mathbf{u}^Q(\mathbf{r}_{2w})$. This condition ensures us that the total flow, the flow due to a free swimmer, and the scattered flow vanish on the wall. In this case, the complete velocity field of a swimmer in the presence of two no-slip walls can be written as $\mathbf{u}(\mathbf{r}) = \mathbf{u}^Q(\mathbf{r}) + \mathbf{u}^{2w}(\mathbf{r})$. What we are interested in is the dynamic influence of the walls on the orientational velocity of the swimmer. The angular velocity of the swimmer due to the interaction with the walls can be obtained as $\dot{\theta} = -\frac{1}{2}\hat{\mathbf{y}}\cdot[\nabla\times\mathbf{u}^{2w}(\mathbf{r})]$. For a swimmer located at a position near the lower wall $z/H \approx 0$, one can expect to obtain the dynamics of the swimmer by considering only the system of images from the nearby wall. For the quadrupole free swimmer defined by the force distribution Eq. (8), a single image quadrupole with $T_{jlm}^I = -f\ell^2\hat{\mathbf{m}}_j\hat{\mathbf{t}}_l\hat{\mathbf{t}}_m$ produces a first approximation to the scattered flow. Here the unit vector $\hat{\mathbf{m}}$ is obtained from $\hat{\mathbf{t}}$ by applying 2θ rotation around the y axis (mirror image with respect to the wall located at $z=0$). The velocity field of such a nondiagonal force quadrupole reads

$$\begin{aligned} \mathbf{u}^{2w} \approx \frac{f\ell^2}{8\pi\eta r^3}\{&[2m_t - 6m_r(\hat{\mathbf{t}}\cdot\hat{\mathbf{r}})]\hat{\mathbf{t}} + [-1+3(\hat{\mathbf{t}}\cdot\hat{\mathbf{r}})^2]\hat{\mathbf{m}} \\ &+ [-6m_t(\hat{\mathbf{t}}\cdot\hat{\mathbf{r}}) - 3m_r + 15m_r(\hat{\mathbf{t}}\cdot\hat{\mathbf{r}})^2]\hat{\mathbf{r}}\}, \end{aligned} \tag{10}$$

where $m_t = \hat{\mathbf{t}}\cdot\hat{\mathbf{m}}$ and $m_r = \hat{\mathbf{r}}\cdot\hat{\mathbf{m}}$. Now having in hand the first approximation to the scattered flow, we can obtain an analytic relation for the swimmer's angular velocity as

$$\dot{\theta} = -\frac{3}{8\pi\eta}\frac{f\ell^2}{z^4}\cos^3\theta. \tag{11}$$

According to this approximate result, for a swimmer moving in the direction $\hat{\mathbf{t}}$ with $\mathcal{V} > 0$, the wall will rotate it in such a way that $\dot{\theta} < 0$. So this swimmer will reorient to decrease its angle with the x axis. Comparing with the full numerical phase diagram in Fig. 2, we see that this approximate analytical result is valid only in a very small part of the phase diagram where

(z/H) and θ are very small parameters. It is interesting that even for small z but for larger θ, one needs to include more images to overcome the no-slip boundary and get the overall correct orientational behavior of the swimmer.

V. SUMMARY AND DISCUSSION

In summary, we have theoretically considered the hydrodynamics of a model active three-bead swimmer moving inside a microfluidic channel. Different types of trajectories for the swimmer are analyzed. The phase diagram for microchannel confinement is in agreement with our previous results for single-wall confinement [6]. Inside the channel, for $\theta > 0$, $\theta < 0$ (but small), and near the wall (small z/H), we recover the same phase behavior as for a single wall. However, for motion far from the channel walls, we can see the effects due to both walls.

It is seen that the hydrodynamic interactions with the walls will eventually lead to nontrivial trajectories for the swimmer. Space-scanning trajectories strongly suggest using the three-bead low Reynolds swimmer as an active mixing device. Flow patterns produced by the motion of this swimmer are also examined by studying the streamlines. Enforcing the system to work in pumping mode does not change the overall face of our results. Mathematically, the difference between the pumping and swimming mode is a change in reference frames. A swimming trajectory in swimming mode corresponds to a far velocity field pattern produced in pumping mode.

[1] E. M. Purcell, Am. J. Phys. **45**, 3 (1977).
[2] J. Happel and H. Brenner, *Low Reynolds Number Hydrodynamics* (Noordhoff, Leyden, 1973).
[3] E. Lauga and T. R. Powers, Rep. Prog. Phys. **72**, 096601 (2009).
[4] S. J. Ebbens and J. R. Howse, Soft Matter **6**, 726 (2010).
[5] Y. Or and R. M. Murray, Phys. Rev. E **79**, 045302 (2009).
[6] R. Zargar, A. Najafi, and M. F. Miri, Phys. Rev. E **80**, 026308 (2009).
[7] A. P. Berke, L. Turner, H. C. Berg, and E. Lauga, Phys. Rev. Lett. **101**, 038102 (2008).
[8] S. E. Spagnolie and E. Lauga, J. Fluid Mech. **700**, 147 (2012).
[9] S. H. Rad and A. Najafi, Phys. Rev. E **82**, 036305 (2010).
[10] T. Brotto, J.-B. Caussin, E. Lauga, and D. Bartolo, Phys. Rev. Lett. **110**, 038101 (2013).
[11] M. C. van Loosdrecht *et al.*, Micro. Rev. **54**, 75 (1990).
[12] J. P. Hernandez-Ortiz, C. G. Stoltz, and M. D. Graham, Phys. Rev. Lett. **95**, 204501 (2005).
[13] E. Lauga *et al.*, Biophys. J. **90**, 400 (2006).
[14] H. Bruus, *Theoretical Microfluidics* (Oxford University Press, Oxford, 2008).
[15] P. S. Dittrich and A. Manz, Nat. Rev. Drug Discovery **5**, 210 (2006).
[16] G. M. Whitesides, Nature (London) **442**, 368 (2006).
[17] H. Chen and J. C. Meiners, Appl. Phys. Lett. **84**, 2193 (2004).
[18] C. C. Chang and R. J. Yang, Microfluid. Nanofluid. **3**, 501 (2007).
[19] T. J. Johnson *et al.*, Anal. Chem. **74**, 45 (2002).
[20] S. C. Jana *et al.*, AIChE J. **40**, 1769 (1994).
[21] A. Rida and M. A. M. Gijs, Anal. Chem. **76**, 6239 (2004).
[22] S. N. Khaderi *et al.*, Lab Chip **11**, 2002 (2011).
[23] J. Toonder *et al.*, Lab Chip **8**, 533 (2008).
[24] J. Hussong *et al.*, Lab Chip **11**, 2017 (2011).
[25] Ph. Marmottant and S. Hilgenfeldt, Proc. Natl. Acad. Sci. USA **101**, 9523 (2004).
[26] M. Leoni *et al.*, Soft Matter **5**, 472 (2009).
[27] E. R. Kay, D. A. Leigh, and F. Zerbetto, Angew. Chem., Int. Ed. **46**, 72 (2007).
[28] V. Balzani *et al.*, Angew. Chem., Int. Ed. **39**, 3348 (2000).
[29] W. F. Paxton *et al.*, J. Am. Chem. Soc. **126**, 13424 (2004).
[30] R. Golestanian and A. Ajdari, Phys. Rev. Lett. **100**, 038101 (2008).
[31] R. Golestanian and A. Ajdari, Phys. Rev. E **77**, 036308 (2008).
[32] L. D. Landau and E. M. Lifshits, *Fluid Mechanics* (Butterworth-Heinemann, Oxford, 1987).
[33] N. Liron and S. Mochon, J. Eng. Math. **10**, 287 (1976).
[34] C. Pozrikidis, *Introduction to Theoretical and Computational Fluid Dynamics* (Oxford University Press, New York, 2011).
[35] J. R. Blake, Proc. Cambridge Philos. Soc. **70**, 303 (1971).